NANO LETTERS

LETTER

pubs.acs.org/NanoLett

Heat Profiling of Three-Dimensionally Optically Trapped Gold Nanoparticles using Vesicle Cargo Release

Anders Kyrsting,[†] Poul M. Bendix,[†] Dimitrios G. Stamou,[‡,§] and Lene B. Oddershede*[,†,§]

[†]Niels Bohr Institute, [‡]Department of Neuroscience and Pharmacology, and [§]Lundbeck Foundation Center for Biomembranes in Nanomedicine, University of Copenhagen, Denmark

Supporting Information

ABSTRACT: Irradiated metallic nanoparticles hold great promise as heat transducers in photothermal applications such as drug delivery assays or photothermal therapy. We quantify the temperature increase of individual gold nanoparticles trapped in three dimensions near lipid vesicles exhibiting temperature sensitive permeability. The surface temperature can increase by hundreds of degrees Celsius even at moderate laser powers. Also, there are significant differences of the heat profiles in two-dimensional and three-dimensional trapping assays.

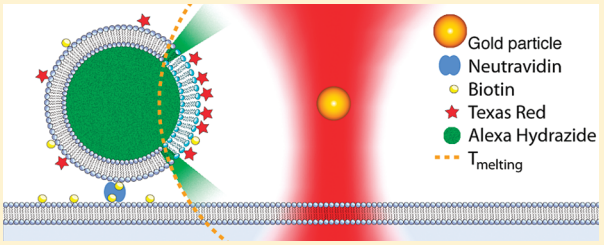

KEYWORDS: Gold nanoparticle, optical tweezers, heating, photothermal therapy, giant unilamellar vesicles, lipid phase transition, surface plasmonics

Irradiation of a metallic nanoparticle results in excitation of surface plasmons giving rise to a significant heating. This effect can be advantageously used in biomedical contexts, for example, for photothermal cancer therapy[1,2] or in nanothermal processing.[3] The fact that a lipid vesicle becomes leaky at the phase transition[4,5] has been used in connection with irradiated gold nanoparticles with the goal of triggering the release of encapsulated molecules .[8−11] Recently, the temperature increase surrounding irradiated gold nanoparticles constrained to two dimensions (2D) through attachment to a supporting membrane was quantified by imaging a local lipid phase transition in the membrane caused by the heated particle.[12,13] Here we show how to quantify the temperature surrounding a gold nanoparticle optically trapped in three dimensions in solution simply by measuring the distance between the particle and a leaking giant unilamellar vesicle (GUV). Comparing the temperature profiles of particles trapped in two[12] or three dimensions reveals that particles are significantly dislocated from the center of the trap during three-dimensional trapping. Moreover, we demonstrate how optical trapping together with fluorescence microscopy can be combined to efficiently probe both permeability and molecular partitioning associated with phase transitions in GUVs, this with potential use for controlled cargo delivery.[14]

Because of their large polarizability, individual metallic nanoparticles in aqueous suspensions are readily trapped by a tightly focused infrared laser beam, an optical trap.[15−19] In the present experiments, gold nanoparticles with diameters between 60 and 200 nm were optically trapped. The optical trap was based on a Spectra Physics J201-BL-106C 1064 nm laser and implemented in a Leica SP5 confocal microscope. A Leica PL APO NA:-1.2 63× water immersion objective was used for all experiments. Gold nanoparticles (British Biocell International) were prepared by sonicating 450 μL from each stock solution. To stabilize the particles, 0.25 mg thiolated PEG (Sigma Aldrich) was added to each suspension and agitated at 1000 rpm for 30 min. The particles were spun down and resuspended in 500 μL Millipore water.

To prepare the lipid bilayers 1-palmitoyl-2-oleoyl-sn-glycero-3-phosphocholine (POPC, item 770557) and 1,2-dipalmitoyl-sn-glycero-3-phosphoethanolamine-*N*-biotinyl (Biotinyl PE, item 870277) lipids from Avanti Polar Lipids each at a concentration of 25 mg/mL were mixed in chloroform at a ratio of (100:1). The 0.4 mL chloroform solution was evaporated in a 5 mL glass vial and placed for two hours in a vacuum desiccator. Lipids were then rehydrated in 3 mL 0.1 M phosphate buffer saline (PBS) overnight (3.3 mg/mL of lipid) and extruded 9 times at a filter pore-size of 100 nm. This stock was used to form supported lipid bilayers in the sample chambers by adding 200 μL of lipid suspension on the glass coverslip and leaving it to settle overnight. The sample chambers were rinsed by flushing 10 times with Millipore water followed by 5 times with 0.1 M PBS. Neutravidin was added to a concentration of 0.2 μM and allowed to bind for 5 min and then washed 5 times with 0.1 M PBS without dehydrating the bilayer.

Giant unilamellar vesicles (GUVs) were formed using 1, 2-dipentadecanoyl-sn-glycero-3-phosphocholine ($DC_{15}PC$, item 850350) and Biotinyl PE, both from Avanti Polar Lipids, and 1, 2-dihexadecanoyl-sn-glycero-3-phosphoethanolamine-Texas Red (TR conjugated PE, item T1395MP) from Invitrogen. They were mixed at the ratios 1000:1:30 in chloroform. One hundred

Received: December 8, 2010

   dx.doi.org/10.1021/nl104280c | *Nano Lett.* XXXX, XXX, 000–000

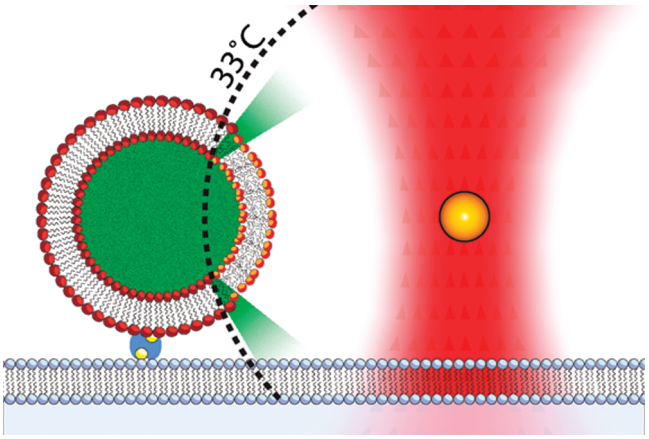

Figure 1. Illustration of the experiment. A GUV containing green membrane impermeant AH is tethered by an avidin−biotin linkage to a bilayer. Heat is radiated from an optically trapped gold nanoparticle moving slowly toward the GUV. The black dashed line indicates the shell around the trapped gold nanoparticle at which the lipid phase transition temperature (33 °C) is reached. At the phase transition temperature, the GUV becomes leaky and green AH diffuses out.

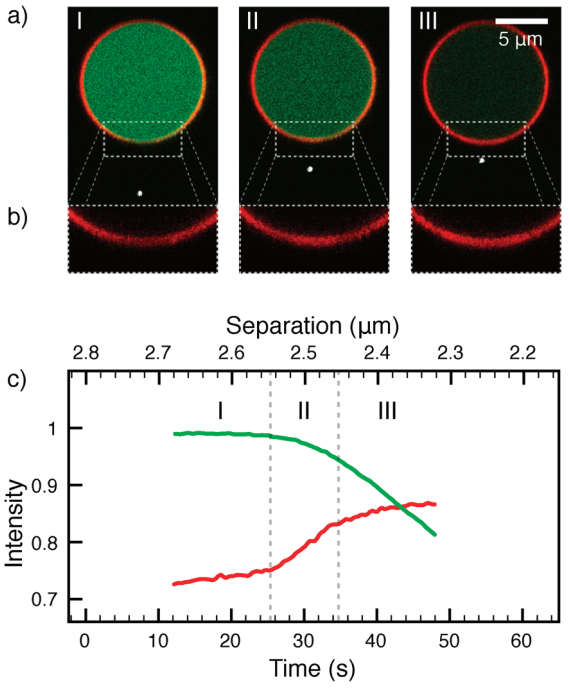

Figure 2. Controlled leakage of a GUV upon approach of an optically trapped gold nanoparticle. (a) Confocal images of a GUV surface (red), its cargo (green), and an optically trapped gold nanoparticle (bright white spot) as the trapped nanoparticle approaches the GUV. (b) Zoom in on the membrane in the boxes of (a). (c) Intensity of the fluorophores in the boxed regions of (a) as a function of traveled distance, the AH signal is normalized by its initial value, the intensity of Texas Red is normalized by the initial AH value. The GUV becomes leaky around $t = 26$ s.

microliters of 25 mg/mL solution was dripped into a custom-made Teflon cylindrical container and allowed to evaporate, followed by 2 h in a vacuum desiccator. Five milliliters of 0.2 M D-Sorbitol was added at 37 °C and the container was kept at 37 °C for 3 h with gentle shaking every 30 min. The suspension was allowed to cool to room temperature and transferred to vials. Encapsulation of Alexa Hydrazide (AH) 488 was performed by adding 10 μL of the dye solution (10 mg/mL in 0.1 M NaCl) to 10 μL of the above GUV solution. This final solution was heat-cycled past the phase transition temperature of the GUV main lipid by leaving it at $T = 37$ °C for 10 min and at 24 °C for 5 min; this procedure was repeated 3 times. The filled GUVs were transferred to the prepared sample chamber immediately after the heat cycle process and left to settle for 30 min. Excess Alexa Hydrazide was washed away very gently using 0.1 M PBS. Deformation of fluid phase GUVs has previously been observed using this tethering strategy[20] but was not observed in this study most likely due to the rigidity of the gel phase GUVs.

At temperatures below the phase transition (33 °C), the membrane of the GUV is impermeable to Alexa Hydrazide; at the phase transition temperature the membrane becomes permeable, thus allowing the fluorophores to diffuse out of the GUV.[5] The cooperativity of the gel to fluid phase transition for the $DC_{15}PC$ bilayer determines the accuracy of our assay. The multilamellar gel to fluid phase transition of this lipid occurs at approximately 33 °C with a half width of less than 0.5 °C (data shown in Supporting Information Figure 1). Small vesicles of the same lipid have a slightly broader phase transition due to curvature stress,[6] and a half width of ~1 °C (data shown in inset of Supporting Information Figure 1). The actual heat capacity of single vesicles has not been measured but previous work using Laurdan fluorophores to measure the hydration of melting GUVs have shown that GUVs have slightly broader phase transitions than multilamellar vesicles,[7] hence, the phase transition characterizing our GUVs probably has a half width of less than 1 °C. The sample chamber was kept at (8 ± 0.5) K below the lipid phase transition temperature. In the experiment, a GUV on the surface was translated at a constant speed of 0.01 μm/s toward an optically trapped gold nanoparticle using a piezo electrical stage with capacitive feedback (PI-P5173CL). The experiment is sketched in Figure 1. The dashed black line in Figure 1 illustrates the shell around the trapped nanoparticle at which the temperature reaches the phase transition temperature causing the green AH inside the GUV to diffuse out of the leaky GUV.

The AH inside the GUV, the Texas Red labeled membrane of the GUV, as well as the optically trapped gold nanoparticle were visualized by confocal microscopy. Alexa Hydrazide 488 was excited at 488 nm and emitted light was collected in the range 495−565 nm. Texas Red DHPE was excited at 594 nm and imaged at 610−710 nm. The gold nanoparticles were imaged using back scattered light from the 594 nm source in the range 589−599 nm. All images were collected simultaneously at 0.78 frames/sec, hence, the bead had moved 12.8 nm with respect to the supported GUV between two consecutive frames. A typical experiment took 40−60 s.

At a critical distance between the optically trapped gold nanoparticle and the surface of the GUV, the GUV became leaky and the AH escaped from the GUV lumen by diffusion through the membrane. This is visualized in Figure 2a, which shows three snapshots during an experiment. The AH inside the GUV is green, the GUV membrane is red, and the trapped gold nanoparticle appears as a bright white spot. In Figure 2a part I, the trapped bead is far away from the GUV and the content of the GUV is intact. In part II, the trapped bead is closer to the membrane, AH is leaking out and the intensity of AH in the lumen has decreased. In part III, the trapped bead is even closer

dx.doi.org/10.1021/nl104280c |*Nano Lett.* XXXX, XXX, 000–000

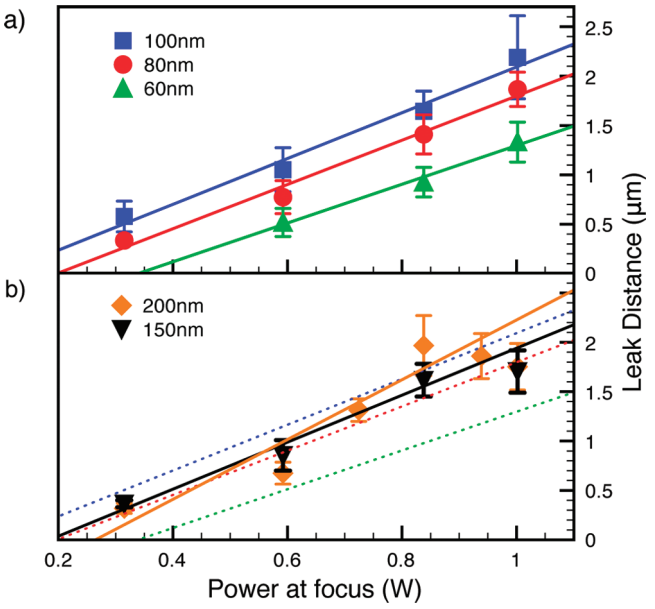

Figure 3. Directly measured leak distance, D, as a function of laser intensity at the sample for gold nanoparticles with diameters 60, 80, and 100 nm (plotted in a); 150 and 200 nm (plotted in b). Lines are linear fits to the data points; color of line refers to particle size.

to the GUV, the encapsulated AH of the GUV has almost completely leaked out. Care was taken to have the optically trapped bead in the same axial height as the equator of the GUV.

Interestingly, the membrane closest to the heated gold nanoparticle shows a local increase in intensity, see Figure 2b. We ascribe this to the partitioning behavior of the TR-DHPE probe into the disordered fluid region that has melted due to the proximity of the trapped particle. Also, it is clear that the membrane did not rupture during the phase transition or while in the fluid phase. Figure 2c quantifies the total intensity of the AH and of the Texas Red as a function of time within the boxed region shown in Figure 2a. Until approximately 26 s had elapsed, there was essentially no change in the AH emission and bleaching was negligible. Then AH started to leak and the lumen intensity decreased in a nearly linear fashion. Simultaneously, the intensity of Texas Red in the membrane region constantly increased. We defined the critical leaking distance as the distance between the trapped gold nanoparticle and the surface of the GUV at the time where a linear fit to the decrease in AH fluorescence intersects with the horizontal line defining the intensity emitted by AH before leakage. The critical leaking distances were measured for a variety of laser powers and particle diameters (60, 80, 100, 150, and 200 nm), and the results are shown in Figure 3. Each point is an average of five independent experiments (different particles), and the error bars denote one standard deviation.

To investigate the possible effect of photobleaching of the AH by the optical trap, a control was performed by trapping a gold nanoparticle inside and near the center of a GUV. Figure 4 shows the AH emission intensity as a function of time. On time scales comparable to and longer than typical experiments, no photobleaching was detected. Hence, the decrease in AH intensity depicted in Figure 2 is not due to photobleaching.

As the gold nanoparticle was located at a distance from any surface that is several orders of magnitude larger than its

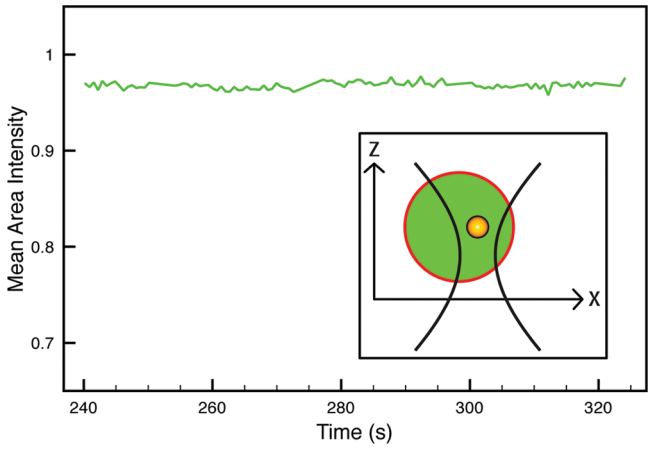

Figure 4. Bleaching of encapsulated AH while a gold nanoparticle was trapped in the center of a GUV (as sketched in the inset). The graph shows the intensity emitted from the AH molecules during 80 s after turning on the optical trap.

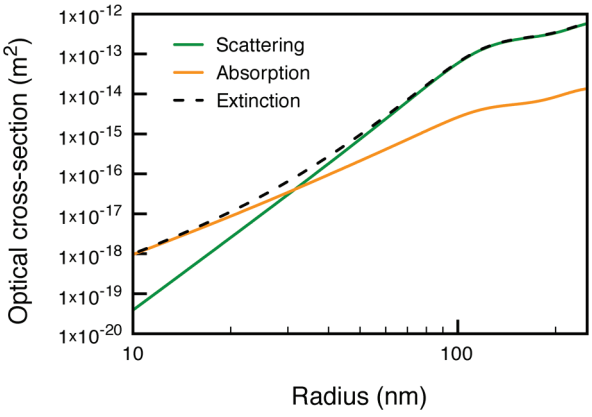

Figure 5. Absorption, scattering, and extinction cross sections for gold particles irradiated by 1064 nm laser light as function of radius, calculated by Mie theory.

diameter, the temperature increase near the particle is well described by the following relation[21]

$$\Delta T(D) = \frac{AR^3}{3K_w D} \quad (1)$$

Here, A is heat input per volume unit, K_w is the thermal conductivity of water, D is the distance from the center of the sphere, and R is the radius of the sphere. $A = IC/V$, where I is the light intensity, C is the absorption cross section, which for these particle sizes is correctly calculated using Mie theory,[22] and V is the particle volume. The absorption, scattering, and extinction cross sections for gold nanoparticles at various radii while irradiated by 1064 nm laser light calculated using Mie theory are shown in Figure 5, though, it might be possible that heating alters the optical properties of the nanoparticle.[23]

For a $\Delta T(D)$ corresponding to the difference between the ambient temperature and the phase transition temperature, eq 1 predicts a linear relationship between leak distance, D, and laser power. This relation is experimentally verified for several particle sizes in Figure 3 where full lines are linear fits to the data points. For particles up to 100 nm, the increase is linear for all

dx.doi.org/10.1021/nl104280c |Nano Lett. XXXX, XXX, 000–000

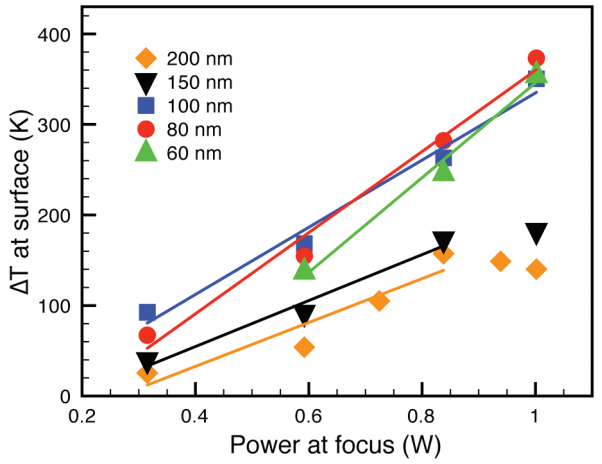

Figure 6. Surface temperature increase, ΔT, of a trapped gold nanoparticles as function of incident laser power. The temperature at the surface is 25 °C + ΔT. The temperature increase is obtained from the measured value of D at the phase transition temperature (Figure 3) and from the inverse relationship between ΔT and D as predicted by eq 1.

intensities investigated (Figure 3a). However, for the two larger particle sizes (150 and 200 nm, shown in Figure 3b) the leaking distance starts to decrease when the power is ramped above 0.9 W, and eq 1 is no longer valid. Hence, the linear fits to the two larges particle sizes, full lines in Figure 3b, are only based on the data points up to 0.9 W. For easy comparison to the other smaller particles, the dotted lines in Figure 3b show the positions of the linear fits to the smaller particles.

Another interesting observation is that for the 60−100 nm particles, the leaking distance increases with particle size, however, for the two larger particles this is not the case. This change in relation between heating, power, and particle size, is probably due to a significant scattering force acting on the large particles at high laser powers, thus causing a displacement of the particle from the trapping focus. Interestingly, these two larger particle sizes have also been reported to have significantly different trapping properties compared to the smaller particles.[16,19]

Using the inverse linear relationship between ΔT and D (from eq 1) and the directly measured value of D, the temperature increase at the surface, ΔT, of the nanoparticle as a function of I can be calculated without detailed knowledge of the additional parameters of eq 1.[12]

The result is shown for five particle sizes in Figure 6. Interestingly, ΔT at the surface of the nanoparticle appears to reach 300 °C, however, without any explosive boiling visible in the microscope. Super heating of water up to 80−90% of the critical temperature of water T_c = 374 °C has been reported in laser heating experiments using pulsed lasers.[24] Boiling must occur at the critical point of water, T_c, where the liquid phase is not stable anymore. We did not see any evidence of boiling around optically trapped particles. However, explosive boiling was observed around particles adhered to a substrate and exposed to high laser powers. The highest temperatures measured in trapped nanoparticles (~300 °C) can be sustained without significant vapor formation due to the energy needed to nucleate a nanoscale bubble on the surface of the particle. The pressure inside a nanoscale bubble of radius r is given by Laplace law $P = 2\sigma/r$ where σ is the surface tension (70 mN/m for air/water interface). This pressure can easily reach tens of bars at which the boiling point of water increases significantly. Finally, the temperature rapidly decays away from the particle thus decreasing the chance of boiling.

The slopes of ΔT versus laser power (plotted in Figure 6 can be used to find the heating at the surface of the particles. We find these values to be 523 K/W for the 60 nm particle, 448 K/W for 80 nm, and 371 K/W for 100 nm, 253 K/W for 150 nm, and 242 K/W for 200 nm, respectively. To our knowledge, these are the first direct measurements of heating associated with a metallic particle optically trapped in 3D. The heating associated with irradiation of a gold nanoparticle embedded in a 2D lipid bilayer reported in ref.[12] is 385 K/W for 80 nm, 452 K/W for 100 nm, 732 K/W for 150 nm, and 1640 K/W for 200 nm, respectively. In ref 25, a more indirect method was used to infer a heating of 266 K/W at the surface of a 3D trapped 100 nm gold nanoparticle, however, this estimate was based on an assumption that the viscosity of the medium was equilibrated with temperature. However, as the temperature gradient is very steep around the particle, the viscosity also has a very steep gradient around the particle that might have led to an underestimation of the surface temperature of the gold nanoparticle. Heating of water at the focus is predicted to be on the order of 1 K/W,[26] while the effective heating by trapped gold nanoparticles is 2 orders of magnitude greater. Thus, the temperature influence from water absorbance in the sample is minimal.

In principle, one can also use eq 1 to theoretically calculate the temperature at the surface of the particle. However, this requires exact knowledge of all parameters entering the equation, for example, of the absorption coefficient, as plotted in Figure 5, and of the light intensity at the particle, I. Many of these parameters are not precisely known. In particular, the exact value of I depends heavily on the axial position of the gold nanoparticle within the trap, a distance that is highly dependent on particle size and yet not reported measured. The strength of our approach is that we directly measure the ratio of all unknown constants in eq 1 and this ratio maps out the heat profile and gives information about the surface temperature of the trapped gold nanoparticle.

There are significant differences between the heating measured from gold nanoparticles trapped in 2D and in 3D. For particles with diameters larger than 80 nm the heating measured from a 2D trapped gold nanoparticle is larger than when the nanoparticle is trapped in 3D and hence free to move (within the trap) in the axial direction. In addition, during 3D trapping the surface temperature decreases with particle size, whereas the surface temperature increases with particle size during 2D trapping. In the 2D trapping assay,[12] the distance between the laser focus and the position of the particle was constant as the trap was positioned with its center at the bead and the bead was confined in the axial direction by the lipid bilayer. In the 2D assay at high laser powers, the particles would blast off the surface into the solution, thus showing that the positioning of a gold nanoparticle in the trap focus is not the equilibrium position.

In the 3D trapping assay, the bead was allowed to move in the axial position to an equilibrium position where the scattering force exerted in the direction of the propagating laser light equated the gradient force exerted by the axially focused laser beam. The larger the scattering force with respect to the gradient force, the further away from the trap center this new equilibrium position is located. Mie theory predicts that the scattering force increases drastically with particle size and eventually becomes dominant over the gradient force, this is shown in Figure 5. Hence, in a 3D trapping assay one would expect the larger particles to be shifted further away from the trap focus in the axial

dx.doi.org/10.1021/nl104280c |Nano Lett. XXXX, XXX, 000–000

direction than the smaller particles. This effect explains the observed difference between 2D and 3D trapping. As the intensity incident on the trapped particle is significantly smaller when the particle is displaced from the center of the tight laser focus, the heating becomes smaller. On the other hand, if the particle is forced to stay in the very center of the focus, as is the case for 2D trapping, then the larger the particle, the larger the heating effect. Future efforts will be devoted to extracting the physical displacement of a metallic particle in an optical trap as a function of size and laser power.

We presented a novel nanoassay where a controlled release of vesicle content was mediated by the heat radiating from an optically trapped gold nanoparticle. The heating of gold nanoparticles optically trapped in three dimensions was directly measured. The temperature increases could be up to 300 °C and were highly dependent on particle size and incident laser power. Surprisingly, the heating of large gold nanoparticles was found to be smaller than the heating of smaller gold nanoparticles. This is probably due to the scattering force, which increases rapidly with particle size and causes the larger particles to be displaced further above the trap focus than the smaller particles. Consequently, heating associated with trapping in 3D differs significantly with respect to trapping in 2D where the particle is confined in the axial direction. We envision this assay to become a useful tool for quantifying temperatures around any type of nanoparticle, e.g., infrared resonant nanoparticles available for photothermal therapy or in drug delivery assays[27] where local heating can be triggered remotely by an external laser.

■ ASSOCIATED CONTENT

Supporting Information. Supplementary Figure 1 depicts the heat capacity of $DC_{15}PC$ lipid bilayers measured using differential scanning calorimetry. The main (blue) graph shows the heat capacity of the multilamellar state. The inset (green graph) shows the heat capacity of small vesicles, extruded using a 50 nm filter, of the same lipid. This material is available free of charge via the Internet at http://pubs.acs.org.

■ AUTHOR INFORMATION

Corresponding Author
*E-mail: oddershede@nbi.dk.

■ ACKNOWLEDGMENT

We acknowledge fruitful discussions with SNS Reihani, Thomas Heimburg for use of his differential scanning calorimetry equipment, and financial support from the University of Copenhagen Excellence grant.

■ REFERENCES

(1) Gobin, A. M.; Lee, M. H.; Halas, N. J.; James, W. D.; Drezek, R. A.; West, J. L. *Nano Lett.* **2007,** *7*, 1929–1934.
(2) Lal, S.; Clare, S. E.; Halas, N. J. *Acc. Chem. Res.* **2008,** *41*, 1842–1851.
(3) Numata, T.; Tatsuta, H.; Morita, Y.; Otani, Y.; Umeda, N. *IEEJ Trans. Electr. Electron. Eng.* **2007,** *2*, 398–401.
(4) Bolinger, P.; Stamou, D.; Vogel, H. *J. Am. Chem. Soc* **2004,** *126*, 8594–8595.
(5) Blicher, A.; Wodzinska, K.; Fidorra, M.; Winterhalter, M.; Heimburg, T. *Biophys. J.* **2009,** *96*, 4581–4591.
(6) Nagano, H.; Nakanishi, T.; Yao, H.; Ema, K. *Phys. Rev. E* **1995,** *52*, 4244–4250.
(7) Bagatolli, L. A.; Gratton, E. *Biophys. J.* **1999,** *77*, 2090–2101.
(8) Needham, D.; Dewhirst, M. *Adv. Drug Delivery Rev.* **2001,** *53*, 285–305.
(9) Pissuwan, D.; Valenzuela, S.; Cortie, M. *Trends Biotechnol.* **2006,** *24*, 62–67.
(10) Pitsillides, C.; Joe, E.; Wei, X.; Anderson, R.; Lin, C. *Biophys. J.* **2003,** *84*, 4023–4032.
(11) Angelatos, A.; Radt, B.; Caruso, F. J. *Phys. Chem. B* **2005,** *109*, 3071–3076.
(12) Bendix, P.; Reihani, S.; Oddershede, L. *ACS Nano* **2010,** *4*, 2256–2262.
(13) Urban, A.; Fedoruk, M.; Horton, M.; Rädler, J. O. *Nano Lett.* **2009,** *9*, 2903–2908.
(14) Wu, G.; Mikhailovsky, A.; Khant, H. A.; Fu, C.; Chiu, W.; Zasadzinski, J. A. *J. Am. Chem. Soc* **2008,** *130*, 8175–8177.
(15) Svoboda, K.; Block, S. *Opt. Lett.* **1994,** *19*, 930–932.
(16) Hansen, P.; Bhatia, V.; Harrit, N.; Oddershede, L. *Nano Lett.* **2005,** *5*, 1937–1942.
(17) Selhuber-Unkel, C.; Zins, I.; Schubert, O.; Sönnichsen, C. S. *Nano Lett.* **2008,** *8*, 2998–3003.
(18) Bosanac, L.; Aabo, T.; Bendix, P.; Oddershede, L. *Nano Lett.* **2008,** *8*, 1486–1491.
(19) Hajizadeh, F.; Reihani, N. *Opt. Express* **2010,** *18*, 551–559.
(20) Bendix, P. M.; Pedersen, M. S.; Stamou, D. *Proc. Natl. Acad. Sci. U.S.A.* **2009,** *106*, 12341–12346.
(21) Goldenberg, H.; Tranter, C. *Br. J. Appl. Phys.* **1952,** *3*, 296–298.
(22) Kreibig, U.; Vollmer, M. *Optical Properties of Metal Clusters*, Springer Series in Materials Science, Vol. 25; Springer: Berlin, 1995.
(23) Palpant, B.; Guillet, Y.; Rashidi-Huyeh, M.; Prot, D. *Gold Bull.* **2008,** *2*, 105–115.
(24) Kotaidis, V.; Dahmen, C.; Plessen, G.; Springer, F.; Plech, A. *J. Chem. Phys.* **2006,** *124*, 184702.
(25) Seol, Y.; Carpenter, A.; Perkins, T. *Opt. Lett.* **2006,** *31*, 2429–2431.
(26) Block, S. *Mod. Cell Biol.* **1990,** *9*, 375–402.
(27) Shi, J.; Votruba, A. R.; Farokhzad, O. C.; Langer, R. *Nano Lett.* **2010,** *10*, 3223–3230.